Dyes and Pigments 195 (2021) 109701

Contents lists available at ScienceDirect

Dyes and Pigments

journal homepage: www.elsevier.com/locate/dyepig

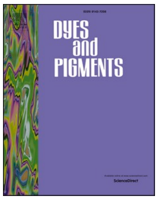

Bright Yb^{3+} complexes for efficient pure near-infrared OLEDs

Mikhail T. Metlin [a,b], Dmitry O. Goryachii [a], Denis F. Aminev [a], Nikolay P. Datskevich [a], Vladislav M. Korshunov [a], Daria A. Metlina [a], Alexander A. Pavlov [c], Lyudmila V. Mikhalchenko [d], Mikhail A. Kiskin [e], Veronika V. Garaeva [c,f], Ilya V. Taydakov [a,*]

[a] P.N. Lebedev Physical Institute of the Russian Academy of Sciences, 53 Leninsky Prospect, 119991, Moscow, Russian Federation
[b] Bauman Moscow State Technical University, 5/1 2-ya Baumanskaya Str, 105005, Moscow, Russian Federation
[c] A.N. Nesmeyanov Institute of Organoelement Compounds of the Russian Academy of Sciences, 28 Vavilova Str, 119991, Moscow, Russian Federation
[d] N.D. Zelinsky Institute of Organic Chemistry of the Russian Academy of Sciences, 47 Leninsky Prospect, 119991, Moscow, Russian Federation
[e] Kurnakov Institute of General and Inorganic Chemistry, Russian Academy of Sciences, 31 Leninskii Prosp, 117901, Moscow, Russian Federation
[f] Moscow Institute of Physics and Technology, 9 Institutskiy per, Dolgoprudny, Moscow Region, 141701, Russian Federation

ARTICLE INFO

Keywords:
Ytterbium
1,3-Diketones
Complexes
NIR OLED
Luminescence

ABSTRACT

A series of neutral Yb^{3+} and Gd^{3+} complexes with isomeric 4,4,4-trifluoro-1-(naphthalenyl)butane-1,3-diones and 1,10-phenanthroline as an ancillary ligand were synthesized and characterized by a full range of analytical methods, including elemental analysis, FTIR and NMR spectroscopy, single crystal X-ray analysis, cyclic voltammetry (CVA) and thermal analysis (TG/DTA). Moreover, the unexpected formation of a mixed diketonate-carboxylate Yb^{3+} complex $[Yb(2\text{-Naph})_2(CF_3COO)(phen)(H_2O)]$ from $[Yb(2\text{-Naph})_3(phen)]$ in solution was observed. The photoluminescence quantum yield (PLQY) for complex $[Yb(2\text{-Naph})_3(phen)]$ in the near infra-red region (one band with a peak at 980 nm) was about 3,2%. This value is close to the highest one reported for 1,3-diketonate complexes of Yb^{3+} ion to date. The energy transfer process is discussed in details, based on the results of TD-DFT calculations and experimental photophysical measurements. These complexes were successfully used as emitters in multilayer OLEDs. The electroluminescence quantum efficiency corresponding to the sole band at 980 nm reached 0.042% with a maximum irradiance of 11 $\mu W/cm^2$ at 8.5 V for $[Yb(2\text{-Naph})_3(phen)]$ based device, which is unusually high for such type of emitters.

1. Introduction

Yb^{3+} coordination compounds demonstrate luminescence in the near-IR region of the spectrum (around 980 nm), and therefore they are widely used for biomedical applications [1–3]; to create UV to NIR radiation converters and intensifiers for silicon photoreceivers [4]; in luminescent thermometry [5,6]; optoelectronics [7]; lasers [8] and for defense applications [9,10]. Trivalent ytterbium is a special ion in the lanthanide series since it has only two 4f levels. Although the Yb^{3+} ion can be directly excited by absorbing radiation at 980 nm, this process is not very efficient. Since f-f electronic transitions are forbidden according to Laporte rule [11]; much more efficient excitation of Yb^{3+} luminescence can potentially be achieved through the use of organic ligands bound to the lanthanide ion. These ligands act as an “antenna” that absorbs light much more efficiently than lanthanide ions and transfers this energy to the excited states of the central Yb^{3+} ion. Various organic and organometallic compounds can be used as a ligands. In particular, macrocyclic ligands [12,13]; heterometallic d-f ensembles [14,15]; carboxylates and phenolates were used as efficient sensibilizers for the Yb^{3+} ion, but the largest number of coordination compounds of ytterbium were obtained with 1,3-diketones [16–19] as the ligands.

Unfortunately, the difference in energies between the triplet level (T_1) of the most common organic ligands and the emission level $^2F_{5/2}$ of the Yb^{3+} ion is too large for efficient energy transfer; therefore, high photoluminescent quantum yields are usually not achieved. In addition, there is no simple empirical rule such as the Latva’s rule [20] that was formulated only for the Eu^{3+} or Tb^{3+} ions. Latva’s empirical rule states that the difference between an energy of the T_1 level of a molecular sensitizer and a lanthanide ion’s excited state should be within the range 2000–4000 cm^{-1} for optimal energy transfer. For the most common ligands, this gap is much wider in Yb^{3+} complexes, since the energy of $^2F_{5/2}$ level is as small as 10400 cm^{-1} [21,22].

---

[*] Corresponding author.
E-mail address: taidakov@gmail.com (I.V. Taydakov).

https://doi.org/10.1016/j.dyepig.2021.109701
Received 23 May 2021; Received in revised form 4 August 2021; Accepted 4 August 2021

Therefore it becomes very important to experimentally select a ligand that would provide the most efficient transfer of the electronic excitation energy to the Yb^{3+} ion. In particular, the multiphonon relaxation should be suppressed to the maximum extent because it leads to nonradiative energy losses [16]. Diketones bearing aromatic and perfluorinated moieties were studied for this purpose before. The aromatic moiety provides a high extinction value of the ligand, while a perfluorinated group makes it possible to reduce multiphonon relaxation, since the phonon energy of the C–F bond is significantly lower than the phonon energy of the C–H bond [23].

Naphthalene 1,3-diketones bearing perfluorinated groups are promising candidates for the synthesis of luminescent ytterbium complexes. The **2-NaphH** ligand (4,4,4-trifluoro-1-(naphthalen-2-yl)butane-1,3-dione) was previously used for the synthesis of luminescent complexes of Eu^{3+} [24,25]; Nd^{3+} [26]; Er^{3+} [27] and some other lanthanides [28–30] or actinides [31] with different ancillary ligands. Surprisingly, an isomeric 1,3-diketone – 4,4,4-trifluoro-1-(naphthalen-1-yl)butane-1, 3-dione (**1-NaphH**) was never previously used as a ligand for the synthesis of any metal complexes. However, up to now, Yb^{3+} ternary complexes with naphthalene diketones were not studied systematically.

The aim of this work is to study the structure and luminescent properties of the tris-β-diketonates of the Yb^{3+} and Gd^{3+} ions with isomeric 4,4,4-trifluoro-1-(naphthalenyl)butane-1,3-diones and some ancillary ligands (1,10-phenanthroline, H_2O). Furthermore, purely NIR-emitting OLEDs based on the Yb^{3+} complexes were fabricated and tested.

2. Experimental

2.1. Materials and methods

The **1-NaphH** and **2-NaphH** ligands were obtained by Claisen condensation of 1- or 2-acetyl naphthalene, respectively, with ethyl trifluoroacetate in the presence of NaH in THF solution, as described earlier [24,32–34]. A representative example of the synthetic procedure is given below. THF was distilled over Na/benzophenone in Ar atmosphere and stored over 3$\mathring{A}$ molecular sieves. MeOH was distilled over Mg turnings and stored over 3$\mathring{A}$ molecular sieves.

Pure salts $YbCl_3 \cdot 6H_2O$ (99.998% trace metals basis) and $GdCl_3 \cdot 6H_2O$ (99.99% trace metals basis) were purchased from Aldrich. All the other reagents were purchased from Aldrich or Acros Organics and used without further purification.

Elemental analysis was performed on Elementar CHNO(S) analyzer. The fluorine content was determined at the Laboratory of Microanalysis of the Nesmeyanov Institute of Organoelement Compounds of the RAS. The europium or gadolinium content was determined by complexometric titration with a standard Trilon B solution in the presence of Xylenol Orange as the indicator. Sample was decomposed by heating with 70% HNO_3 before titration [35].

Single crystal X–ray diffraction data were collected using a Bruker APEX II diffractometer (CCD detector, MoK/α radiation, $\lambda = 0.71073\mathring{A}$) for **[Yb(1-Naph)$_3$(phen)]**, **[Yb(2-Naph)$_3$(phen)]**, **[Yb(2-Naph)$_2$(CF$_3$COO)(phen)(H$_2$O)]**, and **[Gd(1-Naph)$_3$(phen)]**, and a Bruker D8 Venture diffractometer (CCD detector, MoK/α radiation, $\lambda = 0.71073\mathring{A}$) for **[Gd(2-Naph)$_3$(phen)]** [36]. A semiempirical absorption correction was applied for all the compounds [37].

The structures were solved with a ShelXS structure solution program (Olex2 package [38] using direct methods, and refined using a ShelXL [39] refinement package with the least squares minimization in anisotropic approximation for nonhydrogen atoms. Restraints (DFIX, SADI, RIGU, ISOR) were applied during structure refinement. Reflections outside the resolution range (SHEL 30 0.86) were ignored in the refinement for **[Yb(2-Naph)$_3$(phen)]** due to the poor quality of the crystal. The H-atoms were added in the calculated positions and refined using the riding model in isotropic approximation. The crystallographic data for all compounds and the structure refinement statistics are given in Table S1. Atomic coordinates, thermal parameters and bond lengths and angles have been deposited at the Cambridge Crystallographic Data Center (CCDC). Any request to the CCDC for these materials should quote the full literature citation and the reference number CCDC 2041279 (**[Yb(1-Naph)$_3$(phen)]**), 2041278 (**[Yb(2-Naph)$_3$(phen)]**), 2041280 (**[Yb(2-Naph)$_2$(CF$_3$COO)(phen)(H$_2$O)]**), 2041281 (**[Gd(1-Naph)$_3$(phen)]**) and 2041277 (**[Gd(2-Naph)$_3$(phen)]**). These data can be obtained free of charge from The Cambridge Crystallographic Data Center via http://www.ccdc.cam.ac.uk.

Quantum-chemical calculations were performed with the Gaussian 16 Rev A.03 program [40]. DFT (or TD-DFT for exited states) B3PW91/6-311+G(d) level of theory [41,42] was employed for all atoms except lanthanides. Large-core energy-adjusted RECPs for Gd and Yb, developed by the Stuttgart and Dresden teams, along with the accompanying basis set ECP53MWB and ECP59MWB [43]; respectively, were used. In the development of the theoretical models for all the compounds X-ray single crystal structures were used as starting points for geometrical parameters. All calculations were performed for the gas phase. Cartesian coordinates are given in angstroms; absolute energies for all compounds are given in Hartrees. Analysis of vibrational frequencies was performed for all optimized structures. All compounds were characterized only by real vibrational frequencies. The wave function stability was also checked for the ground state of each complex using a stable keyword.

IR absorption spectra of the Yb^{3+} complexes in KBr pellets were recorded with an Infraspec FSM2201 Fourier-transform infrared (FTIR) spectrometer (Infraspec, Russia).

Optical absorption spectra of the Yb^{3+} complexes and the neat ligands were recorded on a Jasco V-770 spectrophotometer in 5×10^{-6} M acetonitrile solutions. HPLC Super Gradient acetonitrile (Panreac, Spain) was used as the solvent. The measurements were performed using quartz cells with 1 cm path length.

NIR photoluminescence and excitation spectra of Yb^{3+} complexes were measured at room temperature by a Horiba Jobin-Yvon Fluorolog FL3-22 spectrofluorimeter using a 450 W xenon arc lamp.

Time-resolved experiments in the NIR region were done with the use of a LeCroy WR62xi digital oscilloscope coupled to a Hamamatsu H10330B-75 InP/InGaAsP photocathode photomultiplier operating in the photon counting mode. A pulsed Nd:YAG laser emitting at 355 nm with a 5 ns pulse duration was used for luminescence excitation.

Triplet level energies of the ligands were determined from the analysis of phosphorescence spectra of the corresponding Gd^{3+} complexes (0-0 transition) recorded at 77 K.

Photoluminescence quantum yields (PLQY) were measured for solid samples by a home-made setup based on a MgO-covered integrating sphere with a diameter of 180 mm and FD-10G calibrated germanium photodiode detector; an CW emitting LED (365 nm) was used as an excitation source. Each sample was measured a few times under slightly different experimental conditions and the results were averaged. The estimated error for the quantum yields was ±10%.

The ^1H NMR spectra and 2D COSY spectra of complexes were recorded with a Bruker Avance 300 FT-NMR spectrometer (^1H frequency of 300.13 MHz). ^1H, ^{13}C NMR spectra and 2D COSY, HMQC and HMBC spectra of ligands were recorded with a Bruker Avance 600 FT-NMR spectrometer (^1H frequency of 600.22 MHz). The NMR chemical shifts (δ, ppm) in ^1H and ^{13}C spectra were determined relative to the residual signals of the CD_2Cl_2 deuterated solvent (^1H 5.32 ppm, ^{13}C 54.00 ppm); the ^{19}F NMR chemical shifts were determined with respect to $CFCl_3$ as the external reference (0.00 ppm).

Cyclic voltammograms (CVs) were recorded with an IPC-Pro potentiostat (Econix, Russia) using a 0.1 M solution of tetrabutylammonium tetrafluoroborate in CH_3CN as the supporting electrolyte. The measurements were done with a glassy carbon working electrode,a platinum grid auxiliary electrode, and a saturated calomel reference electrode connected to the solution in the cell via a ceramic membrane bridge filled with the supporting electrolyte. The peak potentials were determined relative to the redox potential of Fc/Fc$^+$. Ferrocene as an internal standard was added to the solution after recording the curves of the compounds studied. The solution was purged with high purity argon to remove dissolved oxygen. The curves were recorded at a potential sweep rate of 0.1 V^{-1}.

DTA measurements were performed on Shimadzu DTG-60 instrument in air (flow rate 50 mL/min).

NIR electroluminescence spectra were measured at room temperature with an Ocean Optics Maya 2000 Pro CCD spectrometer. The current-voltage characteristics were obtained using two DT 838 Digital multimeters. The luminance of the OLED samples was measured with a TKA-PKM luminance meter produced by TKA Scientific Instruments. The deposition rate was measured in situ by a Leybold Inficon IC-6000 deposition controller calibrated using a NT-MDT atomic force microscope of Integra family.

For all optical measurements, the corresponding instrument response functions were taken into account. The experiments were performed in air under ambient conditions. Degradation of the optical properties was not observed during the experiments.

2.2. Synthesis of ligands and complexes

2.2.1. 4,4,4-Trifluoro-1-(naphthalen-1-yl)butane-1,3-dione (1-NaphH)

Sodium hydride (60% dispersion in mineral oil, 8.0 g, 200 mmol, 4 eqv.) was placed in a three-necked round bottom flask equipped with a magnetic stirring bar, a reflux condenser, a dropping funnel and an argon inlet, and washed with three 50 mL portions of dry hexane to remove the mineral oil. This operation was conducted under argon blanket. Then 100 mL of THF was added and the suspension was stirred for 5 min. A solution of 1-acetylnaphthalene (8.52 g, 50 mmol) and ethyl trifluoroacetate (9.2 g, 7.4 mL, 66 mmol) in 40 mL of dry THF was prepared separately. Approximately 1/15 by volume of this solution was added to the NaH suspension in one portion, followed by addition of 0.5 mL of dry MeOH as the catalyst. The rest of the solution was then added dropwise to maintain a moderate evolution of hydrogen. The resulting dark mixture was stirred for 3 h and left overnight. Next day, 10 mL of dry MeOH was added to the reaction mixture with external cooling by an ice-water bath, followed by addition of 11.5 mL (12 g, 200 mmol) of glacial AcOH. The mixture was evaporated to dryness under diminished pressure, 100 mL of 5% aqueous HCl solution was added, and the diketone was extracted three times with 50 mL portions of EtOAc. The organic phase was washed with water until a neutral pH was obtained, then with 50 mL of brin, and then washed over MgSO$_4$. Evaporation of the solvent gave a solid yellow product. An analytical sample was recrystallized from heptane. M.p. 43–45 °C (lit. 45–48 °C [44].

Light-yellow powder.
Yield – 10.15 g (76%).
For $C_{14}H_9F_3O_2$ (FW 266.22)
Calcd. C, 63.16; H, 3.41;
Found C, 63.29; H, 3.37.

^{1}H NMR (600 MHz, CD_2Cl_2), δ (ppm): 15.22 (br.s., 1H), 8.53 (d, 1H, $^3J_{H-H} = 8.3$ Hz), 8.12 (d, 1H, $^3J_{H-H} = 8.2$ Hz), 7.99 (d, 1H, $^3J_{H-H} = 8.0$ Hz), 7.91 (dd, 1H, $^3J_{H-H} = 6.9$ Hz, $^4J_{H-H} = 1.4$ Hz), 7.68 (ddd, 1H, $^3J_{H-H} = 8.3$ Hz, $^3J_{H-H} = 6.8$ Hz, $^4J_{H-H} = 1.4$ Hz), 7.64 (td, 1H, $^3J_{H-H} = 7.7$ Hz, $^3J_{H-H} = 8.0$ Hz), 7.61 (ddd, 1H, $^3J_{H-H} = 6.9$ Hz, $^4J_{H-H} = 8.2$ Hz), 6.60 (s, 1H);

^{13}C NMR (151 MHz, CD_2Cl_2), δ: 191.5, 174.3 (q, $^2J_{C-F} = 36.6$ Hz), 133.9, 133.7, 132.0, 129.9, 128.8, 128.7, 128.0, 126.8, 125.1, 124.7, 118.4 (q, $^1J_{C-F} = 282.5$ Hz), 97.6 (q, $^3J_{C-F} = 2.2$ Hz).

^{19}F NMR(282 MHz, CD_2Cl_2), δ: −76.53 (s, 3F);

*2.2.2. General method for the preparation of **[Ln(L)$_3$(phen)]** complexes*

To a stirred solution of the corresponding ligand **1-NaphH** or **2-NaphH** (1.5 mmol, 0.4 g) and 1,10-phenanthroline (0.5 mmol, 0.09 g) in 10 mL of an EtOH, a solution of $YbCl_3 \cdot 6H_2O$ (0.5 mmol, 0.194 g) or $GdCl_3 \cdot 6H_2O$ (0.5 mmol, 0.186 g) in 2 mL of hot EtOH was added, followed by dropwise addition of 1 M NaOH solution in EtOH (1.5 mL, 1.5 mmol). A white precipitate formed immediately. The reaction mixture was kept in a closed vial at 45 °C for 3 h with continuous stirring, then cooled to a room temperature. The solid complex was filtered off, washed successively with 5 mL of 50% aqueous EtOH, 10 mL of deionized water, 2 mL of 50% aqueous EtOH, and 5 mL of pentane, and then dried in air. The complexes were purified by recrystallization from hot EtOH and finally dried at 45 °C and 0.1 torr to a constant weight.

Tris-(4,4,4-trifluoro-1-(naphthalen-1-yl)butane-1,3-dionato)(1,10-phenanthroline)ytterbium(III)
[Yb(1-Naph)$_3$(phen)]
Light-yellow powder.
Yield – 0.342 g (59%).
For $C_{54}H_{32}F_9N_2O_6Yb$ (FW1148.86)
Calcd. C, 56.45; H, 2.81; N, 2.44; Yb, 15.06;
Found C, 56.54; H, 2.75; N, 2.49; Yb, 15.17.

Tris-(4,4,4-trifluoro-2-(naphthalen-1-yl)butane-1,3-dionato)(1,10-phenanthroline)ytterbium(III)
[Yb(2-Naph)$_3$(phen)]
Light-yellow powder.
Yield – 0.243 g (42%).
For $C_{54}H_{32}F_9N_2O_6Yb$ (FW1148.86)
Calcd. C, 56.45; H, 2.81; N, 2.44; Yb, 15.06;
Found C, 56.50; H, 2.87; N, 2.53; Yb, 14.96.

Tris-(4,4,4-trifluoro-1-(naphthalen-1-yl)butane-1,3-dionato)(1,10-phenanthroline)gadolinium(III)
[Gd(1-Naph)$_3$(phen)]
White powder.
Yield – 0.447 g (79%).
For $C_{54}H_{32}F_9GdN_2O_6$ (FW1133.07)
Calcd. C, 57.24; H, 2.85; N, 2.47; Gd, 13.88;
Found C, 57.36; H, 2.91; N, 2.40; Gd, 14.09.

Tris-(4,4,4-trifluoro-2-(naphthalen-1-yl)butane-1,3-dionato)(1,10-phenanthroline)gadolinium(III)
[Gd(2-Naph)$_3$(phen)]
White powder.
Yield – 0.414 g (73%).
For $C_{54}H_{32}F_9GdN_2O_6$ (FW1133.07)
Calcd. C, 57.24; H, 2.85; N, 2.47; Gd, 13.88;
Found C, 57.16; H, 2.89; N, 2.52; Gd, 13.97.

2.2.3. General method for the preparation of [Gd(L)$_3$(H$_2$O)$_2$] complexes

To a stirred solution of the corresponding ligand **1-NaphH** or **2-NaphH** (1.5 mmol, 0.4 g) in 10 mL of EtOH, a solution of $GdCl_3 \cdot 6H_2O$ (0.5 mmol, 0.186 g) in 2 mL of hot EtOH was added, followed by dropwise addition of 1 M NaOH solution in EtOH (1.5 mL, 1.5 mmol). The reaction mixture was kept in a closed vial at 45 °C for 6 h with continuous stirring and left at a room temperature overnight. Water (15 mL) was added dropwise with vigorous stirring to the clear mixture, and the resulting emulsion was stirred until a solid precipitate formed (usually 6–10 h). The precipitate was left in the mother liquor overnight, filtered off, washed successively by 5 mL of 50% aqueous EtOH, 10 mL of deionized water, 2 mL of 50% aqueous EtOH and 5 mL of pentane and dried in air. Complexes were purified by recrystallization from hot 50% aqueous EtOH and were finally dried at 45 °C and 0.1 torr to a constant weight. Seeding crystals should be used at this stage to facilitate crystallization of complexes.

Tris-(4,4,4-trifluoro-1-(naphthalen-1-yl)butane-1,3-dionato)(diaqua)gadolinium(III)
[Gd(1-Naph)$_3$(H$_2$O)$_2$]
White powder.
Yield – 0.282 g (57%).
For $C_{42}H_{28}F_9GdO_8$ (FW 988.90)

Calcd. C, 57.24; H, 2.85; N, 2.47; F, 17.29; Gd, 13.88;
Found C, 57.16; H, 2.89; N, 2.52; F,17.36; Gd, 14.09.

Tris-(4,4,4-trifluoro-2-(naphthalen-1-yl)butane-1,3-dionato)(diaqua)gadolinium(III)

[Gd(2-Naph)$_3$(H$_2$O)$_2$]

White powder.
Yield – 0.326 g (66%).
For $C_{42}H_{28}F_9GdO_8$ (FW 988.90)
Calcd. C, 57.24; H, 2.85; N, 2.47; F, 17.29; Gd, 13.88;
Found C, 57.34; H, 2.91; N, 2.39; F,17.12; Gd, 14.17.

2.3. *OLED device fabrication*

2.3.1. *Substrate preparation*

ITO-coated glass substrates with 12 Ohm/sq resistance were purchased from Lumtec (Taiwan). The substrates were successively cleaned by ultrasonication in 15% KOH alcoholic solution, double distilled water, and isopropanol for 15 min each, followed by drying with a dust-free nitrogen flow. The substrates were additionally treated by UV/ozone in a UV-cleaning chamber (Ossila, UK) just before use.

2.3.2. *Deposition of layers*

First, 200 μL of an aqueous solution of PEDOT-PSS film (Lumtec LT-PS001) was spin-coated at 2000 rpm for 1 min onto a freshly cleaned ITO-substrate, and the resulting layer was annealed at 130 °C for 20 min in Ar atmosphere (in a glovebox) to form a 40 nm PEDOT-PSS film. The PVK (Sigma-Aldrich, a hole transport and hole injection layer) was spin-coated from a chlorobenzene solution (5 g/l) directly onto the PEDOT:PSS coated substrate at 2000 rpm followed by drying at 130 °C for 8 min. An active layer of Yb^{3+} complex was thermally evaporated in a vacuum of 10^{-3} Pa from a resistive heated quartz crucible.

An TPBi (Lumtec LT-E302, electron transport layer) was thermally deposited in a vacuum of 10^{-3} Pa. The layer thickness was 18 nm. Finally, a composite cathode consisting of LiF (Lumtec LT-E001, 1 nm) and aluminium (40 nm) was thermally deposited at a rate of 0.2 nm/s through a shadow mask to form four active pixels 12 mm^2.

3. Results and discussion

3.1. *Synthesis of ligands and complexes*

Both ligands were obtained by a modified method previously designed for the preparation of 1,3-diketones, bearing a 2-thienyl or 4-pyrazolyl moieties [45–47]. An excess of NaH (up to 4 molar equivalents with respect to the quantity of the methyl ketone) is important for achieving high yields of 1,3-diketones. Besides, complete evaporation of THF before the extraction of the target diketones increased the yields significantly (up to two times in comparison with the published method for the preparation of the **1-NaphH** ligand [44]. Both diketones obtained were pure enough for the synthesis of complexes.

The heteroleptic complexes (see Fig. 1) were synthesized by the general method described earlier for the corresponding Eu^{3+} [24]; Er^{3+} [29] or Nd^{3+} [26] compounds with the **2-NaphH** ligand and various ancillary ligands, with minor modifications. Surprisingly, no complexes with the **1-NaphH** ligand were described to date. Fortunately, the chemical properties of both isomeric diketones are similar, and the same method is suitable for the preparation of complexes with the **1-NaphH** ligand.

The synthesis of solid hydrated Gd^{3+} complexes is somewhat tricky because they often fail to form crystals. We have tested a few approaches described in literature for the corresponding Eu^{3+} [28] or Er^{3+} compounds [27]; but the results were unsatisfactory. Much better results were obtained by a modified method developed by Carlos et al. [48] for the preparation of hydrated Eu^{3+} complexes with 2-thenoyltrifluoroacetone. Unfortunately, the experimental details are missing in this publication. It was found that solid Gd^{3+} complexes could be readily solidified by precipitation with water from ethanolic solutions and prolonged vigorous stirring of the resulting emulsion at room temperature. The optimal final ratio of EtOH and H_2O in the reaction mixture was around 2:3 v/v. The crystallization takes a few hours. The solid complexes obtained in this way can be purified from hot 50% aqueous EtOH solution.

According to the known literature data, lanthanide complexes with **2-NaphH** ligand and 1,10-phenanthroline are considered to be stable in solutions. However, some fine crystalline matter was precipitated from mother liquor after separation of the main portion of **[Yb(2-Naph)$_3$(phen)]** on keeping for 6 months in a closed vial. These crystals were identified by X-ray diffraction experiment as an unusual mixed

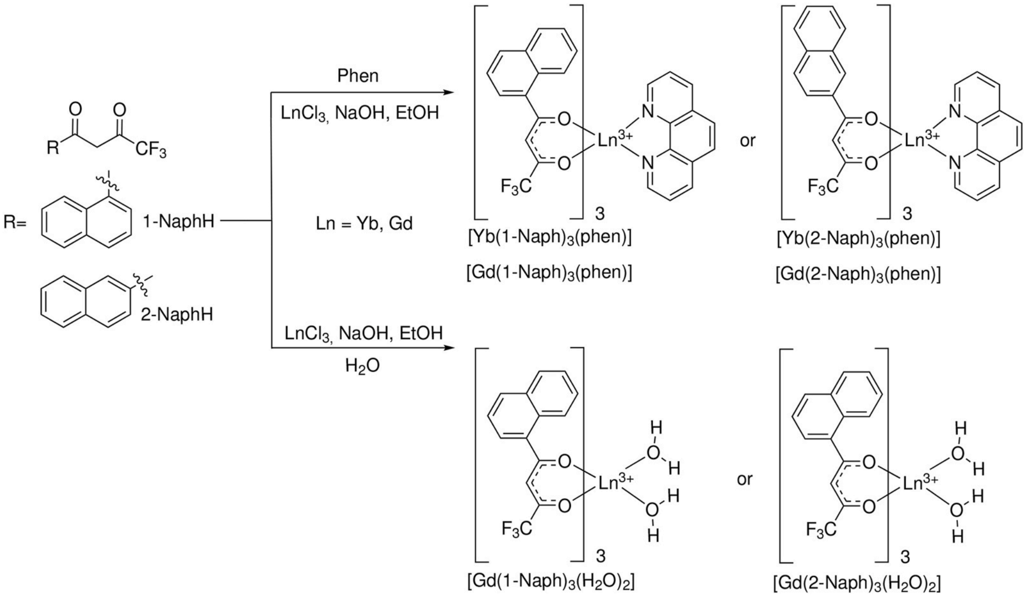

Fig. 1. Synthesis of complexes.

carboxylate-diketonate complex **[Yb(2-Naph)$_2$(CF$_3$COO)(phen)(H$_2$O)]**. The CF_3COO^- anion is coordinated with Yb^{3+} as a k^1–O ligand, so the coordination number of Yb^{3+} equals to 8 and the complex is monomeric (see Fig. 2). Apparently, retro-Claisen degradation of the diketone was the source of the trifluoroacetate anion, but the exact mechanism of its formation is unclear. This anion can be formed during initial deprotonation of the diketone by NaOH or by slow hydrolysis of the neutral **[Yb(2-Naph)$_3$(phen)]** complex in solution. In any case, the yield of this side product was very low, less than 2% (see Fig. 3).

3.2. X-ray crystal structures

The crystals of all the compound are triclinic (space group P-1). **[Yb(2-Naph)$_3$(phen)]** crystalizes as solvate with dichloromethane (**[Yb(L)$_3$(phen)]** $\cdot CH_2Cl_2$), and **[Gd(2-Naph)$_3$(phen)]** as a solvate with 0.4 molecule of trichloromethane (**[Gd(L)$_3$(phen)]** $\cdot$ 0.4CHCl$_3$).

In **[Yb(2-Naph)$_3$(phen)]**, **[Gd(2-Naph)$_3$(phen)]**, **[Yb(1-Naph)$_3$(phen)]**, and **[Gd(1-Naph)$_3$(phen)]**, the lanthanide atom coordinates three chelate 1,3-diketone ligands and one chelate 1,10-phenanthroline molecule (selected bond lengths and angles are listed in Table S2). The main difference between the **[Ln(L)$_3$(phen)]** complexes with **1-NaphH** and **2-NaphH** substituted ligands is the angle between the planes of the naphthyl and 1,3-diketone moieties; in the former, this angle varies from 39° up to 134°, while the latter is almost planar ($10-23°$). The geometry of LnO_6N_2 coordination polyhedra corresponds to a distorted square antiprism for **[Yb(2-Naph)$_3$(phen)]**, **[Yb(1-Naph)$_3$(phen)]**, and **[Gd(1-Naph)$_3$(phen)]**, and a distorted triangular dodecahedron in **[Gd(2-Naph)$_3$(phen)]**.

Compounds **[Yb(2-Naph)$_3$(phen)]** and **[Gd(2-Naph)$_3$(phen)]** are isostructural to the **[Eu(NTA)$_3$(phen)]** $\cdot CH_2Cl_2$ complex reported previously [49].

In molecule of **[Yb(2-Naph)$_2$(CF$_3$COO)(phen)(H$_2$O)]**, the ytterbium atom is coordinated by two chelate 1,3-diketone ligands, one chelate 1,10-phenanthroline molecule, one monodentate trifluoroacetate ligand, and one water molecule (selected bond lengths and angles are listed in Table S2). Two molecules of the complex dimerize due to H-bonding between the hydrogen atoms of the water molecule, the oxygen atoms of 1,3-diketone fragment, and the carboxylate anion (O7–H7A/H7B···O2/O6(1-x,1-y, 1-z): D-H 0.87 Å, H … A 2.23/1.83 Å, D … A 2.963(3)/2.692(3) Å, D-H-A 142°/167°).

In the crystals of all the compounds studied, the aromatic fragments of the ligands in the adjacent molecules interact to form discrete or infinite supramolecular ensembles (more details are provided in Table S3).

3.3. UV–vis absorption spectra

The UV absorption spectra for **[Yb(1-Naph)$_3$(phen)]** and **[Yb(2-Naph)$_3$(phen)]** complexes were recorded in MeCN solution at a ambient temperature (see Fig. 4). They all exhibits the spin-allowed broad bands corresponding to the $\pi \rightarrow \pi^*$ transitions in the ligands.

The observed maxima at 215 and 263 nm can be assigned to the absorption of naphthalene and 1,10-phenanthroline aromatic systems, respectively. The band peaked at 325 nm corresponds to the absorption of the 1,3-diketonate fragment (see Fig. S3 and Table 1). Based on the spectral data, one can conclude that the chemical bonding of ligands with Yb^{3+} ion lead to a dramatic enhancement of the molar extinction. In contrast to the weakly absorbing hydrated Yb^{3+} ion ($\epsilon \sim 10$ M^{-1} cm^{-1}), the molar absorption coefficients for the complexes are 10^3 times higher and reach $2-5 \cdot 10^4$ M^{-1} cm^{-1}.

3.4. FTIR spectra

The FTIR spectra of the Yb^{3+} complexes were recorded within 400–4000 cm^{-1} spectral range (see Fig. 4). The positions of absorption bands are almost the same for all the investigated complexes. Intense absorption of the complexes within 1400–1700 cm^{-1} is associated with the carbonyl groups of the diketone ligand. The absorption bands with maxima at 1134 cm^{-1}, 1200 cm^{-1}, and 1310 cm^{-1} are related to the C–F vibrational transitions. Several bands at 500–900 cm^{-1} are most likely associated with the C–H stretching vibrations in the 1,10-phenanthroline and naphthalene ring. A low-intensity broad band in the 3200–3600 cm^{-1} region indicates presence of water traces in KBr. Significant overlapping of the absorption bands observed within 1100–1700 cm^{-1} range indicates that the complexes have low symmetry.

3.5. Photoluminescence and optical excitation

The emission spectra of the **[Yb(1-Naph)$_3$(phen)]** and **[Yb(2-Naph)$_3$(phen)]** complexes were recorded in MeCN solution at ambient temperature with an excitation in the absorption band ($\pi \rightarrow \pi^*$ transition) of 1,3-diketone (Fig. 5). The emission band is splited into three components, the strongest of which is centered at 976 nm, and two weaker components can be observed, one at 1005 nm and another one at 1034 nm. They were assigned to the $^2F_{5/2} \rightarrow {}^2F_{7/2}$ transition in the Yb^{3+} ion. A similar splitting pattern for Yb compounds was reported previously in the literature [50] and attributed to the ligand-field induced splitting of Yb^{3+} ion energy levels.

The fine structure of the line corresponding to $^2F_{5/2} \rightarrow {}^2F_{7/2}$ transition observed for solid samples (see Fig. S4) differs from that in solutions. It can be attributed to the difference of the geometry of the ligand environment of ytterbium in MeCN solution and in solid state. These geometry changes may be attributed to complex-solvent interactions in solution [51].

Ligand-centered phosphorescence was not observed for the Yb^{3+} complexes at room temperature or at 77 K; this indicates an efficient energy transfer from the excited ligand states to the Yb^{3+} excited level.

The excitation spectra for the solid complexes were recorded at the 980 nm emission band corresponding to the $^2F_{5/2} \rightarrow {}^2F_{7/2}$ transition in Yb^{3+}, see Fig. 5. Intense luminescence was observed only at excitation

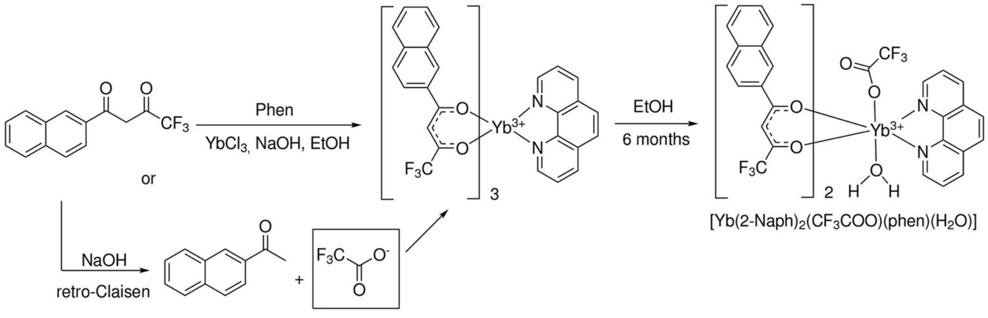

Fig. 2. Formation of Yb^{3+} mixed complex.

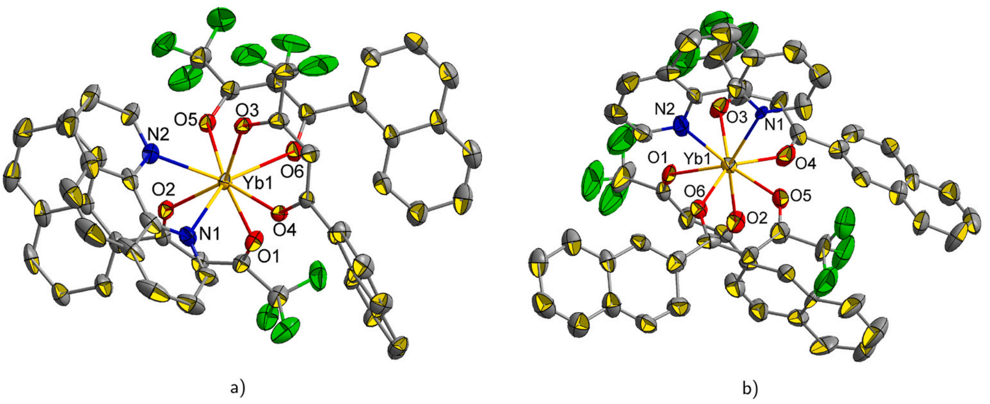

Fig. 3. Crystal structures of complexes **[Yb(1-Naph)$_3$(phen)]** (***a***) and **[Yb(2-Naph)$_3$(phen)]** (***b***).

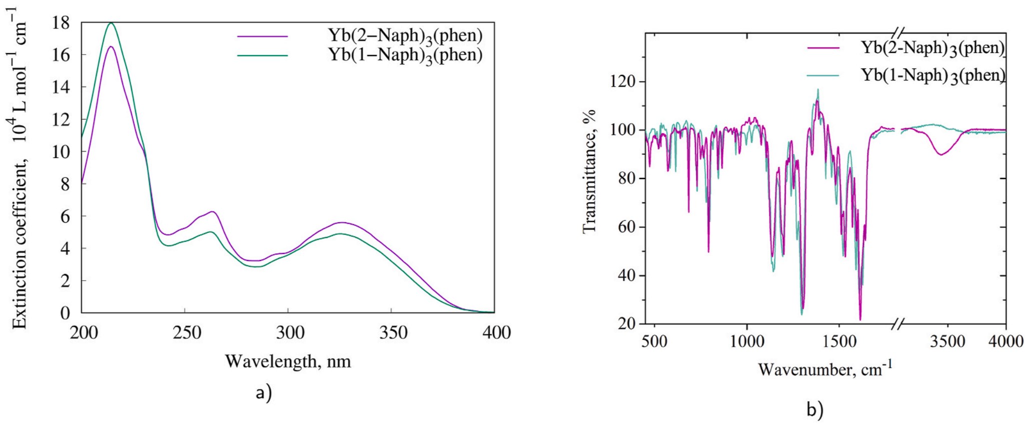

Fig. 4. (***a***) Optical absorption spectra of the **[Yb(1-Naph)$_3$(phen)]** and **[Yb(2-Naph)$_3$(phen)]** complexes in MeCN solutions at ambient temperature; (***b***) FTIR spectra of the investigated Yb^{3+} complexes in KBr pellets.

Table 1
Absorption maxima and $^1S_1$ level energies of the ligands in the Yb^{3+} complexes.

Complex	Extinction, $\times 10^4$ M^{-1} cm^{-1}			$^1S_1$, cm^{-1}
	215 nm	263 nm	325 nm	
Yb(1-Naph)$_3$(phen)	18.4	4.9	4.7	25100
Yb(2-Naph)$_3$(phen)	16.6	7.1	5.4	25800

wavelengths shorter than 400 nm. The excitation spectra qualitatively resemble the absorption spectra in solution. This indicates the absence of strong supramolecular interactions (e.g. π-π stacking, etc.) in the crystals, which would affect the optical properties of the complexes.

Based on the absorption and luminescence excitation data for the complexes studied, one may conclude that ligand-to-metal energy transfer occurs rather efficiently (see Fig. 7). Replacement of water molecules with ancillary ligands (1,10-phenanthroline) provides a well shielded environment around the Yb^{3+} ion that reduces non-radiative processes, and hence increase the emission intensities of the complexes considerably.

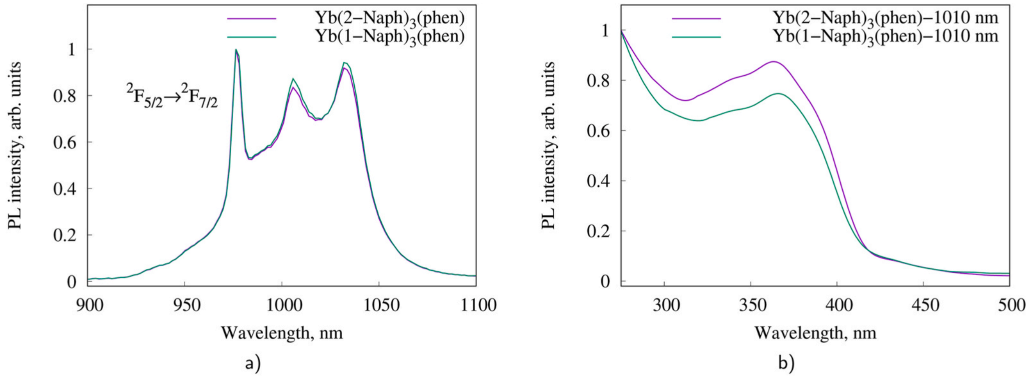

Fig. 5. NIR emission spectra (left panel ***(a)***, $\lambda_{ex} = 365$ nm) of complexes **[Yb(1-Naph)$_3$(phen)]** and **[Yb(2-Naph)$_3$(phen)]** and excitation spectra (right panel ***(b)***, 1010 nm registration) for the same complexes in MeCN solutions at ambient temperature.

3.6. Photoluminescence decays

The photoluminescence decay curves of the Yb^{3+} complexes were recorded at the emission band corresponding to the $^2F_{5/2} \rightarrow {}^2F_{7/2}$ (980–1040 nm) transition. The photoluminescence decays obtained for the **[Yb(1-Naph)$_3$(phen)]** and **[Yb(2-Naph)$_3$(phen)]** complexes in solid phase under 355 nm excitation show a similar behaviour. Kinetic measurements were performed for all three subcomponents of the broad band associated with the $^2F_{5/2} \rightarrow {}^2F_{7/2}$ transition. The photoluminescence decay curves measured for the subcomponent at 1010 nm are presented in Fig. 6. For other subcomponents, the luminescence decays are virtually the same. These decays can be fitted with a biexponential model

$$I_{exp}(t) = \sum_{i=0}^{n} A_i \exp(-t/\tau_i), \tag{1}$$

where A_i are the amplitudes, and τ_i are the characteristic times of the exponential decay components. The decay lifetimes for the solid Yb^{3+} complexes were calculated from the experimental data by means of the Levenberg-Marquardt deconvolution technique [52,53]. The experimental decays can be presented as

$$I_{exp}(t) = \int_0^\infty I_{irf}(t')I_{exp}(t-t')dt'. \tag{2}$$

Here $I_{irf}(t)$ is the instrument response function (IRF). The measured IRF appears to be single-exponential with the corresponding decay time of 1–1.5 ns. The calculated decay times τ_i are listed in Table 2.

Experimental decays in the NIR region were also measured for MeCN solutions of the ytterbium complexes. The results are presented in Fig. S7. For both complexes, the experimental decay curves measured for different emission subcomponents are almost similar and reveal single-exponential behaviour. The long-time components of the biexponential kinetics observed for the solid samples and for the solution are very close to each other (see Table 2 and S4). The nature of short-time components in the biexponential kinetics of solid complexes is unclear. The biexponential model is usually associated with the existence of two independent emission centers in a molecule or crystal, but this hypothesis is not supported by crystallographic data. On the other hand, the kinetics is monoexponential in the solutions. One may conclude that a second emission center probably originates from the defects of crystal packing and they are obviously collapsing upon dissolution of the complex.

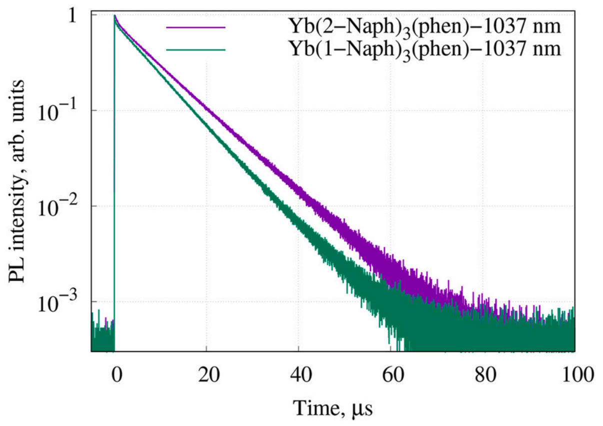

Fig. 6. Luminescence decays of complexes **[Yb(1-Naph)$_3$(phen)]** and **[Yb(2-Naph)$_3$(phen)]** in solid state measured within the band corresponding to the $^2F_{5/2} \rightarrow {}^2F_{7/2}$ transition; $\lambda_{ex} = 355$ nm.

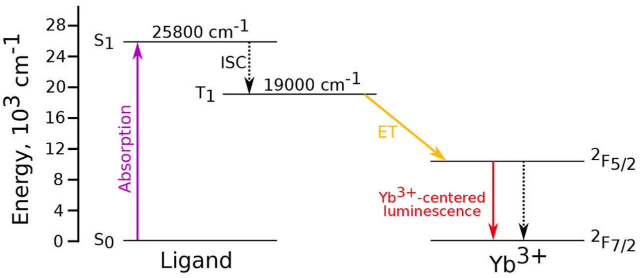

Fig. 7. Energy level diagram for Yb^{3+} complexes; ISC – intersystem crossing, ET – energy transfer.

Table 2
Luminescence decay times τ of Yb^{3+} complexes in solid state obtained for different spectral bands.

Complex	λ, nm	τ_{short}, μs	A_{short}, arb. units	τ_{long}, μs	A_{long}, arb. units
Yb(1-Naph)$_3$(phen)	981	–	–	8.83 ± 0.01	0.97 ± 0.01
	1010	–	–	8.41 ± 0.01	0.97 ± 0.01
	1037	–	–	8.02 ± 0.01	0.97 ± 0.01
Yb(2-Naph)$_3$(phen)	981	–	–	10.93 ± 0.01	0.95 ± 0.01
	1010	0.81 ± 0.02	0.33 ± 0.01	9.16 ± 0.02	0.67 ± 0.01
	1037	0.79 ± 0.02	0.17 ± 0.01	9.62 ± 0.02	0.83 ± 0.01

3.7. Energy transfer

A simplified energy diagram of the levels involved in the energy transfer and radiative relaxation processes is presented in Fig. 7.

After absorption of a photon, an electron transition from the ground singlet state $^1S_0$ to the excited vibrational state $^1S_1^*$ in the organic environment occurs with subsequent relaxation to the lowest excited vibrational state $^1S_1$. The energy of the $^1S_1$ (25800 cm^{-1}) level for each complex was determined from the edges of their optical absorption spectra (see Fig. S5).

Then, there are two possible ways of the $^1S_1 \rightarrow {}^1S_0$ relaxation, the first one by fluorescence with a transition rate of 10^8 s^{-1}, or the second one by a nonradiative process. Additionally, intersystem crossing (ISC) can give rise to transitions from the $^1S_1$ singlet level to the $^1T_1$ triplet level. Generally, the relaxation from $^1T_1$ to $^1S_0$ is forbidden by the selection rules since it requires a spin flip. However, in lanthanide complexes, these selection rules are partially lifted due to the spin–orbit coupling. Therefore, nonradiative and radiative relaxation can take place in the ligand environment; the latter occurs at a rate lower than 10^3 s^{-1}.

The energy of the triplet level of the 1,10-phenanthroline ligand is about 22100 cm^{-1} [54]. The energies of the triplet levels for the **1-NaphH** and **2-NaphH** ligands (~19100 cm^{-1}) were determined from the low-temperature phosphorescence spectra of the corresponding Gd^{3+} complexes. The results of experiments at 77 K are presented in Fig. S6. According to Lewis and Kasha [55]; the position of the triplet level was taken as the maximum of the zero-phonon line. This line corresponds to the highest-energy component in the Gaussian fitting of the spectrum. The calculated data are presented in Table 3. It can be seen that the energy gap between the triplet level of the **1-NaphH** and **2-NaphH** ligands and the resonant level of the Yb^{3+} ions decreases from 8950 to 8700 cm^{-1}, depending on the structure of the naphthalene diketone.

Luminescence of Yb^{3+} is associated with the transition $^2F_{5/2} \rightarrow {}^2F_{7/2}$, see Fig. 7.

Table 3
Triplet level (T_1) energies of the ligands and photoluminescent quantum yields (PLQY) for the Yb^{3+} complexes.

Complex	T_1, cm^{-1}	ΔE, cm^{-1}	PLQY
$Gd(1\text{-}Naph)_3(H_2O)_2$	19030	–	–
$Yb(1\text{-}Naph)_3(phen)$	19220	8950	2.2%
$Gd(2\text{-}Naph)_3(H_2O)_2$	19260	–	–
$Yb(2\text{-}Naph)_3(phen)$	19000	8700	3.2%

ΔE is a gap between the T_1 triplet level and the resonant $^2F_{5/2}$ level of the Yb^{3+} ion.

The low efficiency of the energy transfer to the Yb^{3+} ion in comparision with for example highly luminescent Eu or Tb ions is explained by the difference in energy gap between the triplet level of the **NaphH** ligand and the $^2F_{5/2}$ excited state of Yb^{3+} that is about 10300 cm^{-1}. This value is too high to provide efficient energy transfer without non-radiative energy losses. Unfortunately, this is a fundamental restriction. Furthermore, the relatively low emission intensity of the Yb^{3+} ion in this complex is also due to the presence of C═O oscillators in the first coordination sphere that quench the luminescence to some extent by a nonradiative energy transfer pathway.

Nevertheless, the experimental quantum yield (PLQY) measured for the **[Yb(1-Naph)$_3$(phen)]** and **[Yb(2-Naph)$_3$-(phen)]** complexes in solid state were 2.2% and 3.2%, respectively. These values are among the highest ones reported in the literature to date for diketonates. The quantum yield for **[Yb(2-Naph)$_3$-(phen)]** notably exceeds the values reported for benchmark bright ytterbium emitters **[Yb(tta)$_3$dbso] H$_2$O** (PLQY 1.4%) [56] and **[Yb(tta)$_3$(H$_2$O)$_2$]** (PLQY 0.38%) [57] (see Table 4).

3.8. *DFT calculations*

In order to make an insight into nature of T_1 levels of the Yb^{3+} and Gd^{3+} complexes TD-DFT calculations were performed. The geometries of all complexes were optimized started from the X-ray data. It was found that the lowest energy transition $S_0 \rightarrow T_1$ in all investigated complexes is associated with the transition between HOMO and LUMO, namely from HOMO-2 to LUMO+2 (see Fig. 8 and S8). Both HOMO and LUMO orbitals in complexes **[Gd(1-Naph)$_3$(H$_2$O)$_2$]**, **[Gd(1-Naph)$_3$(phen)]** and **[Yb(1-Naph)$_3$(phen)]** are localized exclusively on diketone ligand, but on different parts of the same molecule. HOMO is located mainly on naphthalene moiety and partially – on diketone fragment, while LUMO is spread along all the molecule, involving CF_3 group. One can note that as far as LUMO is including fluorine atom, CF_3 group has a significant impact on the T_1 state of the **1-NaphH** ligand. The same calculated value of T_1 energy of 19800 cm^{-1} for gadolinium and ytterbium complexes is in a good agreement with the experimental one of 19100 cm^{-1} (see Table 5) measured for the same compounds.

It is worth to mention, that for complex **[Yb(1-Naph)$_3$(phen)]** TD-DFT calculations also revealed an existence of second triplet state $T_1^{'}$. This state is probably associated with the $\pi \rightarrow \pi^*$transition (from HOMO-12 to LUMO+2) in the molecule of 1,10-phenanthroline. The estimated energy of 22763 cm^{-1} for this transition is comparable with the value of 22100 cm^{-1}, reported previously by Biju at al [58]. for T_1 level energy of pure 1,10-phenanthroline. Unfortunately, direct experimental observation of this transition in phosphorescence spectrum of **[Yb(1-Naph)$_3$(phen)]** is quite challenging.

Table 4
Compations of PLQYs measured for different Yb^{3+} complexes.

Complex	PLQY	Source
$Yb(1\text{-}Naph)_3(phen)$	2.2%	current paper
$Yb(2\text{-}Naph)_3(phen)$	3.2%	current paper
$Yb(tta)_3dpso]H_2O$	2.4%	Ahmed, Aderne, Kai, Chavarria and Cremona (2016a)
$Yb(tta)_3dbso]H_2O$	1.4%	Ahmed et al. (2016a)
$Yb(tta)_3(H_2O)_2$	3.2%	Meshkova, Topilova, Bolshoy, Beltyukova, Tsvirko and Venchikov (1999)

Htta - 2-thenoyltrifluoroacetone, dpso - phenyl sulfoxide, dbso - benzyl sulfoxide.

The same calculations were also performed for series of complexes with the isomeric ligand **2-NaphH**. The calculated orbital distribution, orbital contributions into transition $S_0 \rightarrow T_1$ and theoretical values of T_1 and $T_1^{'}$ values were essentially the same (within the calculation error) as for complexes with the ligand **1-NaphH**. For this reason the calculation results for ligand **2-NaphH** are not closely discussed here.

3.9. *Thermogravimetric analysis*

The thermograms (TGA and DTA) of the **[Yb(1-Naph)$_3$(phen)]** and **[Yb(2-Naph)$_3$(phen)]** complexes are shown in Fig. 9. The TG curves of the Yb^{3+} complexes show almost horizontal plots up to 320 °C indicating no weight loss. It proves the thermal stability of the complexes and the absence of occluded solvents. The melting points of the **[Yb(1-Naph)$_3$(phen)]** and **[Yb(2-Naph)$_3$(phen)]** complexes are 214 and 193 °C, respectively. The TG curves of the complexes indicated two successive endothermic processes. The first step of decomposition of **[Yb(1-Naph)$_3$(phen)]** and **[Yb(2-Naph)$_3$(phen)]** occurs at 320 °C with weight loss around 55% and 65%, respectively. The second step was observed at 500 °C for both complexes with 15% and 20% weight loss, respectively. This step is associated with a carbon burning. The combustion finished at 700 °C and YbF_3 is formed as a result of decomposition of both compounds. The superior thermal stability of the novel complexes even in air is extremely important for the preparation of durable OLEDs.

3.10. *NMR spectroscopy*

The ^{1}H, 13C{1H}, 19F{1H} NMR spectra and the 2D COSY, HMQC and HMBC spectra of the ligands (see Fig. S13–S24) were used to assign the NMR signals to the chemical structure. Both diketones are fully enolized in CD_2Cl_2, as it was revealed by NMR spectroscopy. In particular, the signals with an integral intensity of 1H and chemical shifts of $\delta = 6.60$ ppm and 6.81 ppm for **1-NaphH** and **2-NaphH**, respectively, can be attributed to the signals of protons in the $CH = C(OH)CF_3$ moiety. The broad signals at $\delta = 15.22$ ppm in the spectra of the **1-NaphH** ligand and at $\delta = 15.30$ ppm in the spectra of the **2-NaphH** ligand are corresponding to the signals of the OH group in enols.

A significant paramagnetic shift and broadening of signals characteristic for paramagnetic compounds are observed in the ^{1}H NMR spectra and 2D COSY spectra of the Yb^{3+} complexes, see Fig. S25–S30. The broadening of the signals of the protons located closer to the paramagnetic nucleus allows one to distinguish all signals of the 1,10-phenanthroline with the widest signal of the α-proton in the spectra of the complexes. The same regularities hold true for the broadening of the H(6) and H(8) proton signals in the naphthalene moiety. The H(6) proton is sterically closer to the Yb^{3+} ion, which leads to a more intense broadening of its signal. 2D ^{1}H–^{1}H COSY spectra were recorded to confirm the signal assignments. On the whole, the complete sets of NMR data fully confirm the suggested chemical structures of the ligands and Yb complexes in solutions. The integral intensities of signals in ^{1}H NMR spectra match the calculated molecular formulas of the compounds studied.

Unfortunately, the NMR spectra of the Gd^{3+} complexes could not be uninterpreted due to the rapid nuclear relaxation. Only very broad signals without a fine structure were observed.

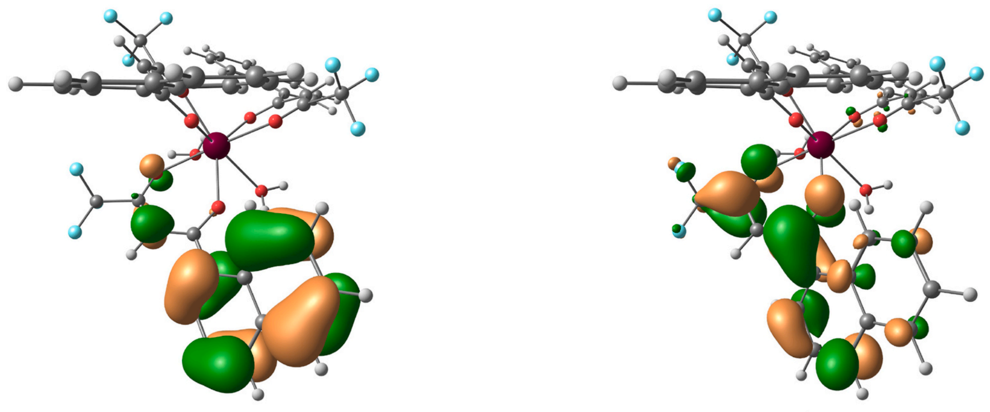
HOMO-2   LUMO+2

Fig. 8. Calculated frontier molecular orbitals HOMO-2 and LUMO+2 for **[Gd(1-Naph)$_3$(H$_2$O)$_2$]** complex.

Table 5
The energies of the first excited triplet state (T$_1$) and first excited singlet state (S$_1$) calculated with 6-311+G(d) basis set. CT corresponds to charge transfer nature of transition.

Complex	Localization	T$_1$, cm^{-1}	Major contribution	S$_1$, cm^{-1}	f	Major contribution
[Gd(1-Naph)$_3$(phen)]	1-NaphH	19821	HOMO-2 → LUMO+2 (65.5%)	24679	0.001	HOMO → LUMO CT(96.5%)
[Gd(1-Naph)$_3$(phen)]	Phen	22763	HOMO-12 → LUMO+2 (51.0%)	–	–	–
[Gd(1-Naph)$_3$(H$_2$O)$_2$]	1-NaphH	19818	HOMO-1 → LUMO+1 (66.4%)	26483	0.015	HOMO → LUMO CT(80.0%)
[Yb(1-Naph)$_3$(phen)]	1-NaphH	19821	HOMO-2 → LUMO+2 (65.2%)	24975	0.001	HOMO → LUMO CT(86.0%)

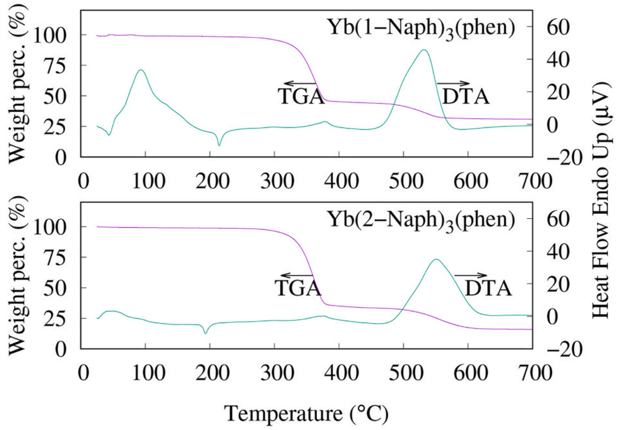

Fig. 9. TGA and DTA plots for complexes **[Yb(1-Naph)$_3$(phen)]** and **[Yb(2-Naph)$_3$(phen)]**.

3.11. Electrochemical properties

The energies of the frontier orbitals were determined using the values of the electrooxidation and electroreduction potentials from the CVs of the **[Yb(1-Naph)$_3$(phen)]** and **[Yb(2-Naph)$_3$(phen)]** complexes. Both compounds evince similar electrochemical properties. The first stages of electroreduction and electrooxidation of the complexes are irreversible at a potential scan rate of 0.1 V^{-1}, see Fig. 10.

The energies of the lowest unoccupied (LUMO) and the highest occupied (HOMO) orbitals were calculated from the magnitude of the electroreduction (E^{red}_{onset}) and electrooxidation (E^{ox}_{onset}) peak onset, respectively. The E^{red}_{onset} and E^{ox}_{onset} values were evaluated relative to the ferrocene/ferrocenium (Fc/Fc$^+$) reversible oxidation potential with an absolute value of −5.1 eV [59]. The HOMO and LUMO values were determined according to Ref. [59] (see, Eqs. (3) and (4)).

$$E_{HOMO}(eV) = -\left(E^{ox}_{onset} + 4.4\ eV\right), \quad (3)$$

$$E_{LUMO}(eV) = -\left(E^{red}_{onset} + 5.1\ eV\right). \quad (4)$$

The results of electrochemical studies are presented in Table 6. The

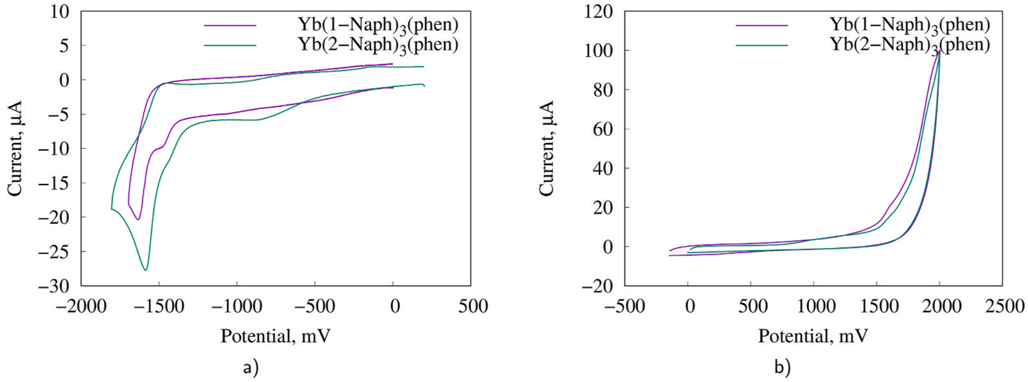

a)   b)

Fig. 10. Electroreduction (***a***) and electrooxidation (***b***) CV plots for complexes **[Yb(1-Naph)$_3$(phen)]** and **[Yb(2-Naph)$_3$(phen)]**.

Table 6
Electrochemical properties of Yb^{3+} complexes in CH_3CN solutions.

Complex	E^{red}_{onset}, V	E^{ox}_{onset}, V	E_{LUMO}, eV	E_{HOMO}, eV	Eg, eV
[Yb(1-Naph)$_3$(phen)]	−1.76	1.08	−3.34	−6.18	2.84
[Yb(2-Naph)$_3$(phen)]	−1.76	1.12	−3.34	−6.22	2.88

experimentally estimated HOMO for **[Yb(1-Naph)$_3$(phen)]** slightly differ from the theoretically estimated one by 0.48 eV ($E^{th}_{HOMO} = -5.60$), whereas the calculated LUMO is higher by 1.17 eV than that obtained from CV data. Both calculated frontier molecular orbitals energies are higher than the experimental ones, and the calculated energy gap is 3.43 eV, in a good accordance with the experimental one of 2.84 eV.

3.12. NIR-OLEDs based on Yb^{3+} complexes

Multilayer OLEDs with the ITO/PEDOT:PSS/PVK/Yb-complex/TPBi/LiF/Al structure were developed based on the **[Yb(1-Naph)$_3$(phen)]** and **[Yb(2-Naph)$_3$(phen)]** complexes as the emitting layer in order to study their electeroluminescence properties. As transport layers, we employed materials suitable for enhancing the efficiency of energy transfer to the luminescent compounds. PEDOT:PSS was used as the hole injection layer, while PVK was used as the hole transport layer. The TPBi electron transport layer also blocked the hole tunneling to the cathode (see Fig. 11).

The switch-on voltage is a crucial characteristic for optimization of the OLED structure. For devices based on the **[Yb(1-Naph)$_3$(phen)]** and **[Yb(2-Naph)$_3$(phen)]** complexes, the switch-on voltage was 8 and 5 V, respectively; these values are rather low and comparable with the lowest operation voltage values reported in the literature for benchmark OLEDs based on Yb^{3+} 1,3-diketonates [60].

Both devices demonstrated electroluminescence solely in the spectral range of 920–1070 nm that is characteristic for the emission of the Yb^{3+} ion. The photoluminescence spectra of the complexes in solid state (see Fig. S4) and the electroluminescence spectra of the developed OLEDs (see Fig. 13 and S12) are essentially the same. This indicates that no change in the chemical composition between the bulk material and the active layer film in the OLED device occurs. It is worth to mentioning that no noticeable electroluminescence in the visible range was observed for OLEDs (see Fig. 13). That means a complete energy transfer from the intermediate layers to the emission layer, with no formation of exciplexes or other unstable emissive species in the interfaces between the layers.

The current-voltage and irradiance-voltage rates are typical of OLEDs (see Fig. 12). The radiant power of 30 μW/cm^2 was measured at a current density of 84 mA/cm^2 for the OLED with the **[Yb(1-Naph)$_3$(phen)]** complex as the emitting layer, while for the **[Yb(2-Naph)$_3$(phen)]** based OLED a radiant power of 11 μW/cm^2 was measured at a current density of 8.5 mA/cm^2. These results are close to the data presented in Ref. [61] with a radiant power of 22 μW/cm^2 for their record-breaking sample. The maximum external quantum efficiency (EQE) of 0.032% was obtained for an OLED based on the **[Yb(1-Naph)$_3$(phen)]** complex and 0.042% for a diode based on the **[Yb(2-Naph)$_3$(phen)]** complex. It is worth mentioning that the EQE values rarely rich the maximum values of 0.15–0.17% [62,63] for the majority of bright Yb^{3+} diketonate based NIR OLEDs.

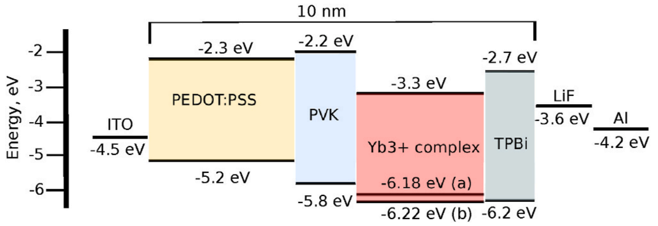

Fig. 11. Energy level diagram of OLED devices. Active layer: complex **[Yb(1-Naph)$_3$(phen)]** (a), **[Yb(2-Naph)$_3$(phen)]** (b).

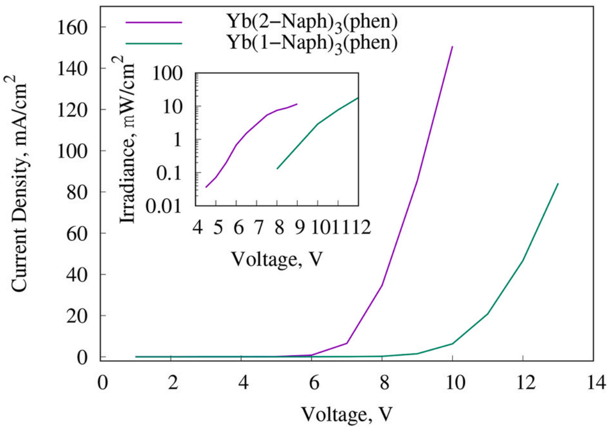

Fig. 12. Irradiance (I) – current density (J) – voltage (V) curves for OLEDs based on complexes **[Yb(1-Naph)$_3$(phen)]** and **[Yb(2-Naph)$_3$(phen)]**.

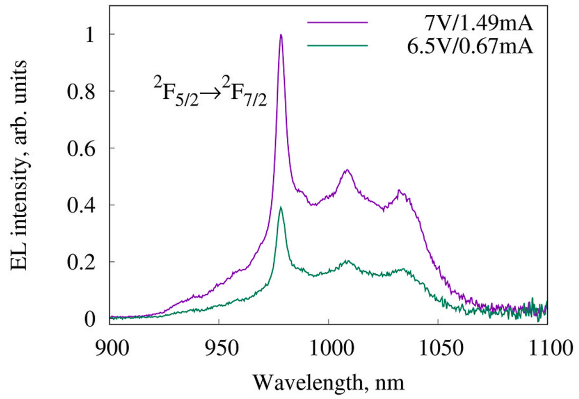

Fig. 13. Electroluminescence spectra of OLED based on complex **[Yb(2-Naph)$_3$(phen)]**.

4. Conclusions

Two novel Yb^{3+} complexes, namely tris-(4,4,4-trifluoro-1-(naphthalen-1-yl)butane-1,3-dionato)(1,10-phenanthroline)ytterbium(III) (**[Yb(1-Naph)$_3$(phen)]**) and tris-(4,4,4-trifluoro-2-(naphthalen-1-yl) butane-1,3-dionato)(1,10-phenanthroline)ytterbium(III) (**[Yb(2-Naph)$_3$(phen)]**) were synthesized and fully characterized. Unusual formation of the mixed carboxylate-diketonate **[Yb(2-Naph)$_2$(CF$_3$COO)(phen)(H$_2$O)]** complex as a side product in the synthesis of neutral tris-complexes was observed and the possible reaction pathways of its formation were discussed.

The photophysical properties of naphthalene based ligands and the corresponding Gd^{3+} and Yb^{3+} complexes were thoroughly studied. The energy of the lowest triplet state T_1 of naphthalene ligands was measured by low temperature (77 K) phosphorescence spectroscopy of the corresponding Gd^{3+} complexes. The intramolecular energy-transfer processes leading to the photoluminescence of the Yb^{3+} compounds were discussed using the experimentally determined HOMO/LUMO energy values and DFT calculations. It was revealed that replacing an **1-NaphH** ligand by an **2-NaphH** ligand resulted in a decrease in the energy gap between the T_1 triplet level and the $^2F_{5/2}$ excited state of the Yb^{3+} ion. A rational choice of the main and ancillary ligands lead to in an increase in the PLQY of the complexes up to 3,2% (for the **[Yb(2-Naph)$_3$(phen)]** complex). It is worthy of note that the new complexes have higher PLQYs values compared to the majority of the previously reported Yb^{3+} complexes with a similar type of the ligand environment.

The Yb^{3+} complexes were successfully used as the near-infrared emitting layer in multi-layer OLEDs. The designed OLED structures are demonstrating characteristic Yb^{3+} electroluminescence with a single emission band in the spectral range of 920–1070 nm with measured maximum EQE values up to 0.04%. Devices based on the **[Yb(2-Naph)$_3$(phen)]** complex have a maximum irradiance of 11 μW/cm^2 at 9 V, which indicates an improvement in the electroluminescence properties over the previously reported devices based on Yb^{3+} complexes with 1,3-diketones.

CRediT authorship contribution statement

Mikhail T. Metlin: Investigation, Data curation, Formal analysis, Writing – original draft. **Dmitry O. Goryachii:** Investigation, Writing – original draft. **Denis F. Aminev:** Investigation. **Nikolay P. Datskevich:** Investigation. **Vladislav M. Korshunov:** Investigation, Formal analysis, Writing – original draft. **Daria A. Metlina:** Formal analysis, Writing – review & editing. **Alexander A. Pavlov:** Investigation, Writing – original draft. **Lyudmila V. Mikhalchenko:** Investigation, Writing – original draft. **Mikhail A. Kiskin:** Investigation, Writing – original draft. **Veronika V. Garaeva:** Investigation. **Ilya V. Taydakov:** Conceptualization, Supervision, Resources, Writing – original draft, Writing – review & editing, Project administration.

Declaration of competing interest

The authors declare that they have no known competing financial interests or personal relationships that could have appeared to influence the work reported in this paper.

Acknowledgements

This work was supported by the Russian Science Foundation (grant No. 19-13-00272). NMR measurements were partially funded by the Council on grants of the President of the Russian Federation (Project MK- 1301.2021.1.3). Luminescent and NMR spectra were measured with financial support from the Ministry of Science and Higher Education of the Russian Federation using the equipment of the Center for molecular composition studies of INEOS RAS. We are grateful to Dr. Alexey Mikhaylov (Kurnakov Institute of General and Inorganic Chemistry) for the performing of TG/DT analysis.

Appendix A. Supplementary data

Supplementary data to this article can be found online at https://doi.org/10.1016/j.dyepig.2021.109701.

References

[1] 1997. SMART (control) and SAINT (integration) Software. Version 5.0. Madison (WI, USA): Bruker AXS.

[2] Ahmed Z, Aderne RE, Kai J, Chavarria HI, Cremona M. Ytterbium β-diketonate complexes for near infra-red organic light-emitting devices. Thin Solid Films 2016; 620:34–42. https://doi.org/10.1016/j.tsf.2016.07.076. doi:10.1016/j.tsf.2016.07.076.

[3] Ahmed Z, Aderne RE, Kai J, Resende JA, Cremona M. Synthesis and NIR-optoelectronic properties of a seven-coordinate ytterbium tris β-diketonate complex with c3 geometrical structure. Polyhedron 2016;117:518–25. https://doi.org/10.1016/j.poly.2016.06.024. doi:10.1016/j.poly.2016.06.024.

[4] Bettencourt-Dias A. Small molecule luminescent lanthanide ion complexes - photophysical characterization and recent developments. Curr Org Chem 2007;11: 1460–80. https://doi.org/10.2174/138527207782418735. doi:10.2174/138527207782418735.

[5] Bhat SA, Iftikhar K. Synthesis and NIR photoluminescence studies of novel yb(III) complexes of asymmetric perfluoryl β-diketone. J Lumin 2019;208:334–41. https://doi.org/10.1016/j.jlumin.2018.12.020. doi:10.1016/j.jlumin.2018.12.020.

[6] Biju S, Raj DA, Reddy M, Kariuki B. Synthesis, crystal structure, and luminescent properties of novel eu3+ heterocyclic β-diketonate complexes with bidentate nitrogen donors. Inorg Chem 2006;45:10651–60.

[7] Biju S, Raj DBA, Reddy MLP, Kariuki BM. Synthesis, crystal structure, and luminescent properties of novel eu^{3+} heterocyclic β-diketonate complexes with bidentate nitrogen donors. Inorg Chem 2006;45:10651–60. https://doi.org/10.1021/ic061425a. doi:10.1021/ic061425a.

[8] Borda P, Crease A, Legzdins P. The determination of lanthanides in organometallic complexes by the closed oxygen flask method. Microchem J 1973;18:172–7. https://doi.org/10.1016/0026-265x(73)90100-8. doi:10.1016/0026-265x(73)90100-8.

[9] Bünzli JCG. On the design of highly luminescent lanthanide complexes. Coord Chem Rev 2015;293–294:19–47. https://doi.org/10.1016/j.ccr.2014.10.013. doi:10.1016/j.ccr.2014.10.013.

[10] Bünzli JCG. Rising stars in science and technology: luminescent lanthanide materials. Eur J Inorg Chem 2017;2017:5058–63. https://doi.org/10.1002/ejic.201701201. doi:10.1002/ejic.201701201.

[11] Cardona CM, Li W, Kaifer AE, Stockdale D, Bazan GC. Electrochemical considerations for determining absolute frontier orbital energy levels of conjugated polymers for solar cell applications. Adv Mater 2011;23:2367–71. https://doi.org/10.1002/adma.201004554. doi:10.1002/adma.201004554.

[12] Carlos L, Fernandes J, Ferreira RS, Malta O, Gonçalves I, Ribeiro-Claro P. Emission quantum yield of a europium(III) tris-β-diketonate complex bearing a 1, 4-diaza-1, 3-butadiene: comparison with theoretical prediction. Chem Phys Lett 2005;413: 22–4. https://doi.org/10.1016/j.cplett.2005.07.033. doi:10.1016/j.cplett.2005.07.033.

[13] Chiu HC, Lee SL, Kapuriya N, Wang D, Chen YR, Yu SL, Kulp SK, Teng LJ, Chen CS. Development of novel antibacterial agents against methicillin-resistant staphylococcus aureus. Bioorg Med Chem 2012;20:4653–60. https://doi.org/10.1016/j.bmc.2012.06.018. doi:10.1016/j.bmc.2012.06.018.

[14] Cotman AE, Cahard D, Mohar B. Stereoarrayed CF3 -substituted 1, 3-diols by dynamic kinetic resolution: ruthenium(II)-catalyzed asymmetric transfer hydrogenation. Angew Chem Int Ed 2016;55:5294–8. https://doi.org/10.1002/anie.201600812. doi:10.1002/anie.201600812.

[15] Dolg M, Stoll H, Savin A, Preuss H. Energy-adjusted pseudopotentials for the rare earth elements. Theor Chim Acta 1989;75:173–94. https://doi.org/10.1007/bf00528565. doi:10.1007/bf00528565.

[16] Dolomanov OV, Bourhis LJ, Gildea RJ, Howard JAK, Puschmann H. OLEX2: a complete structure solution, refinement and analysis program. J Appl Crystallogr 2009;42:339–41. https://doi.org/10.1107/s0021889808042726. doi:10.1107/s0021889808042726.

[17] Fondo M, Corredoira-Vázquez J, García-Deibe AM, Sanmartín-Matalobos J, Amoza M, Botas AMP, Ferreira RAS, Carlos LD, Colacio E. Field-induced slow magnetic relaxation and luminescence thermometry in a mononuclear ytterbium complex. Inorg. Chem. Front. 2020;7:3019–29. https://doi.org/10.1039/d0qi00637h. doi:10.1039/d0qi00637h.

[18] Francis B, Nolasco MM, Brandão P, Ferreira RAS, Carvalho RS, Cremona M, Carlos LD. Efficient visible-light-excitable eu^{3+} complexes for red organic light-emitting diodes. Eur J Inorg Chem 2020;2020:1260–70. https://doi.org/10.1002/ejic.202000027. doi:10.1002/ejic.202000027.

[19] Frisch MJ, Trucks GW, Schlegel HB, Scuseria GE, Robb MA, Cheeseman JR, Scalmani G, Barone V, Petersson GA, Nakatsuji H, Li X, Caricato M, Marenich AV, Bloino J, Janesko BG, Gomperts R, Mennucci B, Hratchian HP, Ortiz JV, Izmaylov AF, Sonnenberg JL, Williams-Young D, Ding F, Lipparini F, Egidi F, Goings J, Peng B, Petrone A, Henderson T, Ranasinghe D, Zakrzewski VG, Gao J, Rega N, Zheng G, Liang W, Hada M, Ehara M, Toyota K, Fukuda R, Hasegawa J, Ishida M, Nakajima T, Honda Y, Kitao O, Nakai H, Vreven T, Throssell K, Montgomery Jr JA, Peralta JE, Ogliaro F, Bearpark MJ, Heyd JJ, Brothers EN, Kudin KN, Staroverov VN, Keith TA, Kobayashi R, Normand J, Raghavachari K, Rendell AP, Burant JC, Iyengar SS, Tomasi J, Cossi M, Millam JM, Klene M, Adamo C, Cammi R, Ochterski JW, Martin RL, Morokuma K, Farkas O, Foresman JB, Fox DJ. Gaussian 16 revision A.03. Wallingford CT: Gaussian Inc; 2016.

[20] Sheldrick GM. SADABS, program for scanning and correction of area detector data. Göttingen (Germany): Univ. of Göttingen; 2004.

[21] Hasegawa Y, Sugawara T, Nakanishi T, Kitagawa Y, Takada M, Niwa A, Naito H, Fushimi K. Luminescent thin films composed of nanosized europium coordination polymers on glass electrodes. ChemPlusChem 2015;81:187–93. https://doi.org/10.1002/cplu.201500382. doi:10.1002/cplu.201500382.

[22] Hasegawa Y, ichi Tsuruoka S, Yoshida T, Kawai H, Kawai T. Enhanced deep-red luminescence of tris(hexafluoroacetylacetonato)samarium(III) complex with phenanthroline in solution by control of ligand coordination. J Phys Chem 2008; 112:803–7. https://doi.org/10.1021/jp075855d. doi:10.1021/jp075855d.

[23] Henderson B, Imbusch GF. Optical spectroscopy of inorganic solids, vol. 44. Oxford University Press; 2006.

[24] Jin GQ, Ning Y, Geng JX, Jiang ZF, Wang Y, Zhang JL. Joining the journey to near infrared (NIR) imaging: the emerging role of lanthanides in the designing of molecular probes. Inorg. Chem. Front. 2020;7:289–99. https://doi.org/10.1039/c9qi01132c. doi:10.1039/c9qi01132c.

[25] Jinnai K, Kabe R, Adachi C. A near-infrared organic light-emitting diode based on an yb(iii) complex synthesized by vacuum co-deposition. Chem Commun 2017;53: 5457–60. https://doi.org/10.1039/c7cc01580a. doi:10.1039/c7cc01580a.

[26] Keller C, Schreck H. Die chelatbildung und extraktion des dreiwertigen actiniums, americiums, curiums und californiums mit acetylaceton und einigen seiner derivate. J Inorg Nucl Chem 1969;31:1121–32. https://doi.org/10.1016/0022-1902(69)80161-2. doi:10.1016/0022-1902(69)80161-2.

[27] Korshunov V, Ambrozevich S, Taydakov I, Vashchenko A, Goriachiy D, Selyukov A, Dmitrienko A. Novel β-diketonate complexes of eu^{3+} bearing pyrazole moiety for bright photo- and electroluminescence. Dyes Pigments 2019;163:291–9. https://doi.org/10.1016/j.dyepig.2018.12.006. doi:10.1016/j.dyepig.2018.12.006.

[28] Latva M, Takalo H, Mukkala VM, Matachescu C, Rodríguez-Ubis JC, Kankare J. Correlation between the lowest triplet state energy level of the ligand and lanthanide(III) luminescence quantum yield. J Lumin 1997;75:149–69. https://doi.org/10.1016/s0022-2313(97)00113-0. doi:10.1016/s0022-2313(97)00113-0.

[29] Lenaerts P, Driesen K, Deun RV, Binnemans K. Covalent coupling of luminescent tris(2-thenoyltrifluoroacetonato)lanthanide(III) complexes on a merrifield resin. Chem Mater 2005;17:2148–54. https://doi.org/10.1021/cm0486868. doi:10.1021/cm0486868.

[30] Lewis GN, Kasha M. Phosphorescence and the triplet state. J Am Chem Soc 1944;66:2100–16.

[31] Li J, Kong M, Yin L, Zhang J, Yu F, Ouyang ZW, Wang Z, Zhang YQ, Song Y. Photochemically tuned magnetic properties in an erbium(III)-based easy-plane single-molecule magnet. Inorg Chem 2019;58:14440–8. https://doi.org/10.1021/acs.inorgchem.9b01831. doi:10.1021/acs.inorgchem.9b01831.

[32] Li Z, Zhang H, Yu J. Near-infrared electroluminescence from double-emission-layers devices based on ytterbium (III) complexes. Thin Solid Films 2012;520:3663–7. https://doi.org/10.1016/j.tsf.2011.12.052. doi:10.1016/j.tsf.2011.12.052.

[33] Linden-Leibeszeit JBS, Eliseeva SV, Chaudhary N, Zeller M, Petoud S, Trivedi ER. Near-infrared emitting heterobimetallic zn-4f schiff base complexes with visible excitation wavelength. Eur J Inorg Chem 2019;2020:75–8. https://doi.org/10.1002/ejic.201901042. doi:10.1002/ejic.201901042.

[34] Mara D, Artizzu F, Laforce B, Vincze L, Hecke KV, Deun RV, Kaczmarek AM. Novel tetrakis lanthanide β-diketonate complexes: structural study, luminescence properties and temperature sensing. J Lumin 2019;213:343–55. https://doi.org/10.1016/j.jlumin.2019.05.035. doi:10.1016/j.jlumin.2019.05.035.

[35] Maron L, Eisenstein O. Do f electrons play a role in the lanthanide-ligand bonds? A DFT study of Ln(NR$_2$)$_3$; R = H, SiH$_3$. J Phys Chem 2000;104:7140–3. https://doi.org/10.1021/jp0010278. doi:10.1021/jp0010278.

[36] Marquardt DW. An algorithm for least-squares estimation of nonlinear parameters. J Soc Ind Appl Math 1963;11:431–41.

[37] Martín-Ramos P, da Silva PSP, Lavín V, Martín IR, Lahoz F, Chamorro-Posada P, Silva MR, Martín-Gil J. Structure and NIR-luminescence of ytterbium(iii) beta-diketonate complexes with 5-nitro-1, 10-phenanthroline ancillary ligand: assessment of chain length and fluorination impact. Dalton Trans 2013;42:13516. https://doi.org/10.1039/c3dt51376a. doi:10.1039/c3dt51376a.

[38] Meshkova SB, Topilova ZM, Bolshoy DV, Beltyukova SV, Tsvirko MP, Venchikov VY. Quantum efficiency of the luminescence of ytterbium(III) ß-diketonates. Acta Phys Pol, A 1999;95:983–90. https://doi.org/10.12693/APhysPolA.95.983.

[39] Metlina D, Metlin M, Ambrozevich S, Taydakov I, Lyssenko K, Vitukhnovsky A, Selyukov A, Krivobok V, Aminev D, Tobokhova A. Luminescence and electronic structure of nd3+ complex with pyrazole-substituted 1, 3-diketone and 1, 10-phenanthroline. J Lumin 2018;203:546–53. https://doi.org/10.1016/j.jlumin.2018.07.005. doi:10.1016/j.jlumin.2018.07.005.

[40] Ning Y, Cheng S, Wang JX, Liu YW, Feng W, Li F, Zhang JL. Fluorescence lifetime imaging of upper gastrointestinal pH in vivo with a lanthanide based near-infrared τ probe. Chem Sci 2019;10:4227–35. https://doi.org/10.1039/c9sc00220k. doi:10.1039/c9sc00220k.

[41] Peng XX, Zhu XF, Zhang JL. Near infrared (NIR) imaging: exploring biologically relevant chemical space for lanthanide complexes. J Inorg Biochem 2020;209:111118. https://doi.org/10.1016/j.jinorgbio.2020.111118. doi:10.1016/j.jinorgbio.2020.111118.

[42] Petrova O, Taydakov I, Anurova M, Akkuzina A, Avetisov R, Khomyakov A, Mozhevitina E, Avetissov I. Luminescent hybrid materials based on an europium organic complex and borate glasses. J Non-Cryst Solids 2015;429:213–8. https://doi.org/10.1016/j.jnoncrysol.2015.09.012. doi:10.1016/j.jnoncrysol.2015.09.012.

[43] Press WH, Teukolsky SA, Vetterling WT, Flannery BP. Numerical recipes in c++. The art of scientific computing 1992;2:1002.

[44] Qi Y, Sun O, Zhou Y, Yao Y, Cheng Z, Gao T, Li H. Enhanced near-infrared luminescence in ln2cd2 (ln = nd, yb) heterotetranuclear complexes. CrystEngComm 2020;22:3287–93. https://doi.org/10.1039/d0ce00341g. doi:10.1039/d0ce00341g.

[45] Qiu H, Chen G, Sun L, Hao S, Han G, Yang C. Ethylenediaminetetraacetic acid (EDTA)-controlled synthesis of multicolor lanthanide doped BaYF5 upconversion nanocrystals. J Mater Chem 2011;21:17202. https://doi.org/10.1039/c1jm12950c. doi:10.1039/c1jm12950c.

[46] de Sá G, Malta O, de Mello Donegá C, Simas A, Longo R, Santa-Cruz P, da Silva E. Spectroscopic properties and design of highly luminescent lanthanide coordination complexes. Coord Chem Rev 2000;196:165–95. https://doi.org/10.1016/s0010-8545(99)00054-5. doi:10.1016/s0010-8545(99)00054-5.

[47] Sabea HA, Norel L, Galangau O, Roisnel T, Maury O, Riobé F, Rigaut S. Efficient photomodulation of visible eu(III) and invisible yb(III) luminescences using DTE photochromic ligands for optical encryption. Adv Funct Mater 2020;30:2002943. https://doi.org/10.1002/adfm.202002943. doi:10.1002/adfm.202002943.

[48] Santos HP, Gomes ES, dos Santos MV, D'Oliveira KA, Cuin A, Martins JS, Quirino WG, Marques LF. Synthesis, structures and spectroscopy of three new lanthanide β-diketonate complexes with 4, 4′-dimethyl-2, 2′-bipyridine. near-infrared electroluminescence of ytterbium(III) complex in OLED. Inorg Chim Acta 2019;484:60–8. https://doi.org/10.1016/j.ica.2018.09.030. doi:10.1016/j.ica.2018.09.030.

[49] Sheldrick GM. A short history ofSHELX. Acta Crystallogr. A Found. Crystallogr. 2007;64:112–22. https://doi.org/10.1107/s0108767307043930. doi:10.1107/s0108767307043930.

[50] Subhan MA, Rahman MS, Alam K, Hasan MM. Spectroscopic analysis, DNA binding and antimicrobial activities of metal complexes with phendione and its derivative. Spectrochim Acta Mol Biomol Spectrosc 2014;118:944–50. https://doi.org/10.1016/j.saa.2013.09.110. doi:10.1016/j.saa.2013.09.110.

[51] Taidakov IV, Zaitsev BE, Lobanov AN, Vitukhnovskii AG, Datskevich NP, Selyukov AS. Synthesis and luminescent properties of neutral eu(III) and gd(III) complexes with 1-(1, 5-dimethyl-1h-pyrazol-4-yl)-4, 4, 4-trifluoro-1, 3-butanedione and 4, 4, 5, 5, 6, 6, 6-heptafluoro-1-(1-methyl-1h-pyrazol-4-yl)-1, 3-hexanedione. Russ J Inorg Chem 2013;58:411–5. https://doi.org/10.1134/s0036023613040190. doi:10.1134/s0036023613040190.

[52] Taydakov IV, Akkuzina AA, Avetisov RI, Khomyakov AV, Saifutyarov RR, Avetissov IC. Effective electroluminescent materials for OLED applications based on lanthanide 1.3-diketonates bearing pyrazole moiety. J Lumin 2016;177:31–9. https://doi.org/10.1016/j.jlumin.2016.04.017. doi:10.1016/j.jlumin.2016.04.017.

[53] Taydakov IV, Korshunov VM, Belousov YA, Nelyubina YV, Marchetti F, Pettinari R, Pettinari C. Synthesis, crystal structure and photophysical properties of mixed-ligand lanthanide complexes with 1, 3-diketonates bearing pyrazole moieties and 1, 10-phenanthroline. Inorg Chim Acta 2020;513:119922. https://doi.org/10.1016/j.ica.2020.119922. doi:10.1016/j.ica.2020.119922.

[54] Taydakov IV, Kreshchenova YM, Dolotova EP. A convenient and practical synthesis of β-diketones bearing linear perfluorinated alkyl groups and a 2-thienyl moiety. Beilstein J Org Chem 2018;14:3106–11. https://doi.org/10.3762/bjoc.14.290. doi:10.3762/bjoc.14.290.

[55] Taydakov IV, Zaitsev BE, Krasnoselskiy SS, Starikova ZA. Synthesis, x-ray structure and luminescent properties of sm3+ ternary complex with novel heterocyclic β-diketone and 1, 10-phenanthroline (phen). J Rare Earths 2011;29:719–22. https://doi.org/10.1016/s1002-0721(10)60529-7. doi:10.1016/s1002-0721(10)60529-7.

[56] Ullmann S, Hahn P, Mini P, Tuck KL, Kahnt A, Abel B, Suburu MEG, Strassert CA, Kersting B. Mixed-ligand lanthanide complexes supported by ditopic bis(imino-methyl)-phenol/calix[4]arene macrocycles: synthesis, structures, and luminescence properties of [ln2(l2)(MeOH)2] (ln = la, eu, tb, yb). Dalton Trans 2020;49:11179–91. https://doi.org/10.1039/d0dt02303e. doi:10.1039/d0dt02303e.

[57] Wang L, Zhao Z, Wei C, Wei H, Liu Z, Bian Z, Huang C. Review on the electroluminescence study of lanthanide complexes. Adv. Opt. Mater. 2019;7:1801256. https://doi.org/10.1002/adom.201801256. doi:10.1002/adom.201801256.

[58] Willauer AR, Palumbo CT, Fadaei-Tirani F, Zivkovic I, Douair I, Maron L, Mazzanti M. Accessing the +IV oxidation state in molecular complexes of praseodymium. J Am Chem Soc 2020;142:5538–42. https://doi.org/10.1021/jacs.0c01204. doi:10.1021/jacs.0c01204.

[59] Wu J, Li HY, Xu QL, Zhu YC, Tao YM, Li HR, Zheng YX, Zuo JL, You XZ. Synthesis and photoluminescent properties of series ternary lanthanide (eu(III), sm(III), nd (III), er(III), yb(III)) complexes containing 4, 4, 4-trifluoro-1-(2-naphthyl)-1, 3-butanedionate and carbazole-functionalized ligand. Inorg Chim Acta 2010;363:2394–400. https://doi.org/10.1016/j.ica.2010.03.067. doi:10.1016/j.ica.2010.03.067.

[60] Yao W, Tian Q, Liu J, Xue Q, Li M, Liu L, Lu Q, Wu W. Preparation and RGB upconversion optic properties of transparent anti-counterfeiting films. Nanoscale 2017;9:15982–9. https://doi.org/10.1039/c7nr05744j. doi:10.1039/c7nr05744j.

[61] Zhang JX, Chan WL, Xie C, Zhou Y, Chau HF, Maity P, Harrison GT, Amassian A, Mohammed OF, Tanner PA, Wong WK, Wong KL. Impressive near-infrared brightness and singlet oxygen generation from strategic lanthanide–porphyrin double-decker complexes in aqueous solution. Light Sci Appl 2019;8. https://doi.org/10.1038/s41377-019-0155-9. doi:10.1038/s41377-019-0155-9.

[62] Zhang X, Liu L, Yu C, Li H, Fu G, Lü X, Wong WK, Jones RA. Highly efficient near-infrared (NIR) luminescent tris- β -diketonate yb^{3+} complex in solution and in PMMA. Inorg Chem Commun 2016;70:153–6. https://doi.org/10.1016/j.inoche.2016.06.006. doi:10.1016/j.inoche.2016.06.006.

[63] Zucchi G, Maury O, Thueŕy P, Ephritikhine M. Structural diversity in neodymium bipyrimidine compounds with near infrared luminescence: from mono- and binuclear complexes to metal-organic frameworks. Inorg Chem 2008;47:10398–406. https://doi.org/10.1021/ic800967x. doi:10.1021/ic800967x.